Nuclear Physics A396(1983)319c-328c.

EVOLUTION OF NUCLEAR SHAPES IN $^{157-161}$Yb AS A FUNCTION OF SPIN AND NEUTRON NUMBER

M. Jääskeläinen*, D. G. Sarantites, F. A. Dilmanian, R. Woodward and H. Puchta**

Department of Chemistry, Washington University, St.Louis, Missouri 63130 U.S.A.

and

J. R. Beene, J. Hattula*, M. L. Halbert, D. C. Hensley and J. H. Barker††

Oak Ridge National Laboratory, Oak Ridge, Tennessee 37830 U.S.A.

The population distributions of the entry states, the entry lines $\langle E^* \rangle$ versus multiplicity, the energy spectra and the angular distributions of the continuum γ-rays as a function of multiplicity in $^{157-161}$Yb from the reactions of 136 MeV and 149 MeV ^{20}Ne with ^{144}Nd and ^{146}Nd have been investigated with a 4π multidetector system gated with a Ge detector. The observed entry lines and γ-decay modes indicate changes in the nuclear structure with increasing spin. This systematic change for N = 87 - 91 Yb isotopes suggests an evolution of nuclear shapes from prolate at low spins to particle aligned oblate structure for ^{157}Yb and ^{158}Yb followed by the onset of high-K bands built on largely deformed oblate states at increasingly higher spin between 38 and 50 $\hbar$ with increasing neutron number for $^{157-161}$Yb. Furthermore evidence for an evolution to triaxial shape at I $\simeq$ 50 for ^{158}Yb was found.

1. Introduction

The behavior of nuclei at high angular momenta has been the prime interest in experimental heavy-ion physics[1]) and the focus of theoretical discussions[2]) for almost two decades. The combination of new heavy-ion beams and sophisticated experimental instrumentation are the tools, which are used to investigate the nuclei at high spin. Multidetector arrays of up to fourteen NaI detectors[3-6]) were used first, and more recently, good efficiency γ-ray coincidence-sum spectrometers[7,8]) and correlation techniques[9]) have been employed. The rare earth nuclei with neutron number $\sim$ 90 have been investigated and discussed more extensively.

The evolution of nuclear structure as a function of angular momentum and proton or neutron number is of fundamental importance in understanding the interplay of the collective and single particle degrees of freedom which determines nuclear behavior away from closed shells. Experimentally only a few nuclei have been found to obtain an oblate ground state. With increasing angular momentum, however, an alignment of quasiparticle angular momenta tends to make the nucleus oblate. The nuclei around A = 150 are known to have few-particle yrast states up to I $\simeq$ 38 with a small oblate deformation ($\varepsilon \sim 0.1 - 0.2$)[10]). This behavior is well understood also with the rotating liquid drop model[11]), which predicts the evolution of nuclear shapes with increasing angular momentum from spherical, at I = 0, to increasingly deformed oblate structure up to I $\sim$ 70 (for A = 160). This behavior is expected to be strongly modified by the shell structure of the nuclei.

* Present address: Department of Physics, University of Jyväskylä, Jyväskylä, Finland.
** Present address: Department of Physics, University of Münich, Münich, West Germany
† Oak Ridge Associated Universities Research Participant on leave from St.Louis University, St.Louis, MO 63103. Present address: South Carolina Electric and Gas Company, Columbia, SC 29218.

For nuclei A $\geq$ 160 the pairing effects at low spins cause the significant prolate deformations ($\varepsilon \sim 0.1 - 0.3$) observed. The exitation energy and angular momentum are then generated by collective rotation around an axis perpendicular to the symmetry axis. However, with increasing rotational frequency, the pairing can be broken and a few particles align their spin vectors along the rotation axis. These effects cause the backbending phenomenon[1]) and can break the axial symmetry, but the nuclei retain basically prolate shape ($\gamma \simeq 0^{\circ}$)[12]). Alignment of additional particles and the rotation can increase the shell energy for prolate shape and finally lead to an oblate nucleus rotating around the symmetry axis. Thus the tendency for prolate nuclei to become oblate with increasing angular momentum is a combined liquid drop and shell effect. For nuclei with N > 90 the negative shell energy for prolate shape is so strong that a transition from prolate to oblate shape is not likely[13]). The good rotational behavior of those nuclei is also experimentally observed up to spin $\sim$ 65 $\hbar$. Thus the nuclei with N $\simeq$ 85 - 90 on the border of the deformation region are the most probable canditates for such a change. Recently several theoretical calculations for Er and Yb nuclei have been performed [14-16]).

Transitions from one type of nuclear structure to another can be observed in a single nucleus as a function of spin. For the yrast states and the states near the yrast line these effects should vary in a systematic way with neutron (or proton) number. The observation of both the change and its systematics is of fundamental importance in understanding the phenomenon. Here evidence for an evolution of nuclear shapes with increasing spin in the N = 87-91 Yb isotopes is presented.

2. Experimental methods

Metallic targets of ^{144}Nd and ^{146}Nd were bombarded with 136 MeV and 149 MeV ^{20}Ne beams from ORIC. The triggering signal for the electronics of the Spin Spectrometer, a 4π multidetector system, was derived from a Ge detector positioned at 117° to the beam. In the data analysis the exit channels were selected by gating on known low lying gamma transitions in each product nucleus. In these experiments 69 out of 72 NaI detectors (92.3 % of 4π) in the spectrometer were used. For each event the Ge pulse height and its time relative to the cyclotron RF and all non-zero pulse heights from the NaI detectors and their times relative to the Ge trigger were recorded. The event tapes were first processed to correct for non-linearities in the NaI pulse heights, match the gains of the NaI elements, derive an accurate reference time for each event by averaging the times of the NaI γ-pulses, and separate neutron and γ-ray pulses by time of flight. The processed events were then sorted to construct the desired spectra.

2.1 ENTRY STATE MEASUREMENTS

The final events were first sorted to construct a Ge spectrum for each γ-ray coincidence fold (k) and each 1.0 MeV interval in total γ-ray pulse height (H). The areas of the Ge peaks due to the $2^+ - 0^+$ or $17/2^+ - 13/2^+$ yrast transitions in $^{157-161}$Yb from each spectrum were determined by least-squares fits with Gaussian peak shapes to provide the population distribution, $Q_x(H,k)$, for each exit channel x. Alternately, gates on these transitions and nearby background were placed on the Ge pulse height and the events were scanned to produce the $Q_x(H,k)$ distributions directly. The same results were obtained from both methods. The entry state populations, $R_x(E^*,M_\gamma)$, in exitation energy-multiplicity space were obtained from the measured distributions $Q_x(H,k)$ by an iterative least-squares unfolding procedure[17,18]). Some of the angular momentum and exitation energy is removed by low energy or delayed transitions (below the gating transition) that were not detected by the spectrometer. The M_γ and E^* distributions for these cannels have been shifted to compensate for these undetected transitions[18]). The response functions of the spectrometer, $P(E^*,M_\gamma \rightarrow H,k)$, used in the unfolding procedure were constructed from data taken with radioactive sources as descriped in ref. [17]).

2.2 GAMMA-RAY DECAY MEASUREMENTS

The γ-ray decay of the entry states was studied using the NaI detectors in the spectrometer. The pulse height spectra for each coincidence fold, k, were constructed from five different groups of detectors at angles of 24.4°, 45.6°, 65.7°, 77.5° and 87.3° (and their suplements) with respect to the beam. These spectra were constructed in coincidence with the $2^+ - 0^+$ or $17/2^+ - 13/2^+$ yrast transitions in the product nuclei observed in the Ge detector and corrected for the underlying Compton background in the Ge gate. The NaI pulse height spectra were then unfolded to yield the γ-ray energy spectra, by an iterative unfolding procedure that corrects for the responses of the detectors. These were obtained from measurements with radioactive sources of γ-ray energies between 136 keV and 4439 keV and included the effects of detector to detector scattering and coincidence summing appropriate for each pulse height spectrum[17]). The associated multiplicities for each spectrum (or coincidence fold) were determined from the spectrometer response functions, $P(E^*,M_\gamma \rightarrow H,k)$, and the deduced entry state populations, $R_x(E^*,M_\gamma)$, as described in detail in ref. [17]).

3. Experimental results

3.1 POPULATION OF THE ENTRY STATES

The entry state populations, $R_x(E^*,M_\gamma)$, were determined for all xn and αxn channels from 136 MeV and 149 MeV ^{20}Ne + ^{146}Nd reactions and 149 MeV ^{20}Ne + ^{144}Nd reaction. Some of the results from ^{20}Ne + ^{146}Nd reaction at 136 MeV are illustrated in Fig. 1a which shows the experimental $Q_{6n}(H,k)$ distribution for ^{160}Yb. Contour maps of the unfolded entry state populations, $R_x(E^*,M_\gamma)$, from the xn channels are shown in Fig. 1b.

The Monte Carlo code JULIAN-PACE[19]) modified to include a more realistic treatment of γ-ray strengths was used to carry out the statistical model calculations. The initial ℓ distributions were assumed to be of the form

$$(2\ell+1)(1 + \exp\frac{\ell-\ell_{fus}}{d})^{-1}.$$

Reasonable agreement with the experiment was obtained with $\ell_{fus} = 59.5$ and $d = 1$. This is a close approximation to that predicted by the sum rule model [20]). The level density parameter used in the calculations was $a = A/9.5$. The yrast lines were taken from the rotating liquid drop model above spin 22; below spin 22 the moment of inertia was assumed to decrease linearly with decreasing spin to approximate the behavior of rotational nuclei. The E1 γ-ray emission strength function included the giant dipole resonance with shape parameters taken from experimental systematics and strength determined by the energy-weighted sum[18]). Statistical E2 and M1 transitions were included with B(E2) = 1.0 W.u. and B(M1) = 0.005 W.u. together with collective stretched E2 transitions with B(E2) = 100 W.u. below $E_\gamma = 2$ MeV. With these parameters the Monte Carlo γ-cascades proceeded to the vicinity of the yrast line and then were assumed to reach the ground state or an yrast state with spin < 2 by stretched E2 transitions[14]). The theoretical entry state distributions were constructed in (E^*,I)-space and (E^*,M_γ)-space with these calculations. The optimum parameters were obtained by comparing the experimental and calculated $R_x(E^*,M_\gamma)$ distributions.

The main features of the entry state populations such as the position of the entry lines, the shapes of the E^* and M_γ projections, and the cross-sections of individual exit channels are reproduced well by the performed statistical calculations. The Figs. 1c and 1d show the calculated entry state populations for the xn cannels from ^{20}Ne + ^{146}Nd reaction at 136 MeV. The measured and calculated entry lines from the data of Fig. 1 are compared in Fig. 2a. A good agreement is observed for the positions and the slopes of the main part of the entry lines. At higher multiplicities the experimental data show a significant decrease in the slope of the entry lines for ^{160}Yb and ^{161}Yb at $M_\gamma \simeq 25$ and 28 , respectively. The same decrease in the slopes of the entry lines is observed at $M_\gamma \simeq 25$ for ^{160}Yb and at $M_\gamma \simeq 23$ for ^{159}Yb in the entry lines from ^{20}Ne + ^{146}Nd reaction at

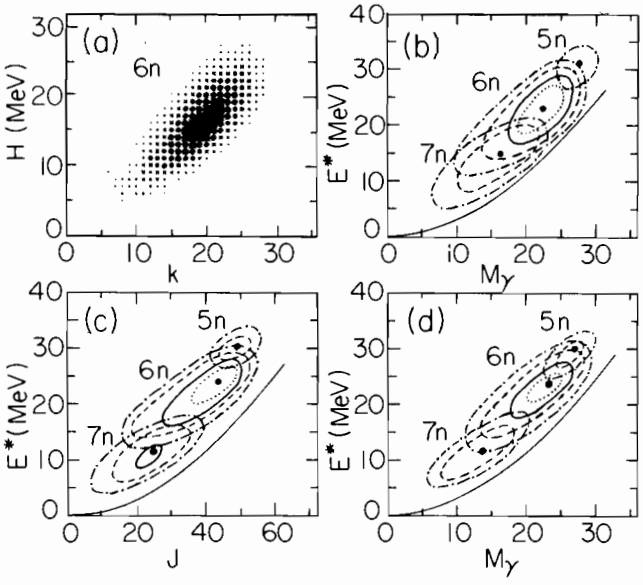

Fig. 1 Entry state population distributions for xn products from 136 MeV ^{20}Ne on ^{146}Nd. (a) Experimental $Q_{6n}(H,k)$ distribution for ^{160}Yb. Contour maps of (b) experimental entry state populations $R_\gamma(E^*,M_\gamma)$, (c) calculated entry state populations in (E^*,J) space and (d) calculated entry state populations in (E^*,M_γ) space for the xn channels. The cross-section contours are for factors 1.4, 2.0, 4.0 and 8.0 relative to the peak value of 6n channel and are given by the dotted, full, dashed, and dash-dotted curves, respectively. The heavy dots indicate the location of the maximum intensity for each channel. The ^{160}Yb yrast line used in the calculation is shown by the curve below the contours.

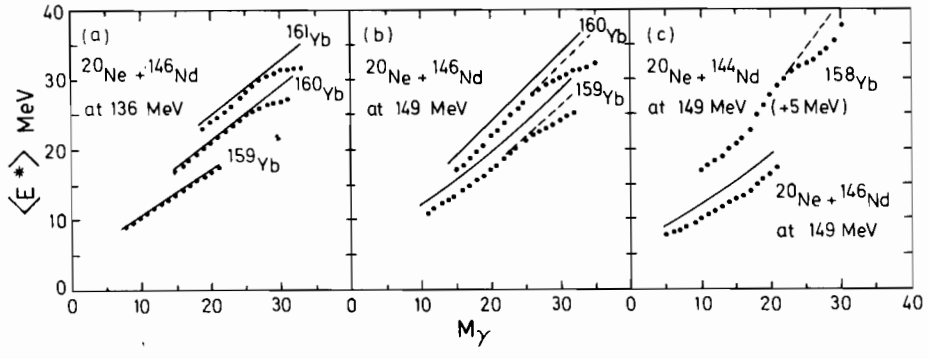

Fig.2 Experimental (data points) and calculated (solid lines) entry lines $\langle E^* \rangle$ versus multiplicity, M_γ, for the $^{159-161}$Yb isotopes from (a) 136 MeV and (b) 149 MeV ^{20}Ne on ^{146}Nd reactions, and (c) for ^{148}Nd from 149 MeV ^{20}Ne on ^{144}Nd and ^{146}Nd reactions. The dashed lines were drawn parallel to the calculated entry lines.

149 MeV which are shown in fig. 2b. Fig. 2c shows the entry lines for ^{158}Yb from ^{20}Ne + ^{144}Nd and ^{20}Ne + ^{146}Nd reactions at 149 MeV. In this case the decrease in the slope of the entry line occurs at $M_\gamma \simeq 22$. These effects observed in the experimental entry lines cannot be reproduced by the statistical model calculations with any reasonable variation of the parameters that does not involve the onset of a different nuclear structure or a rapid increase in the effective moment of inertia of the product nuclei. These two effects should be reflected in a different way in the decay of the entry states and thus by studying the associated γ-ray spectra they can be distinguished.

3.2 DECAY OF THE ENTRY STATES

Some unfolded γ-ray energy spectra from all the NaI detectors in the spectrometer normalized to their associated multiplicities are shown in fig. 3. The spectra from ^{161}Yb (fig. 3a) evolve in a familiar way for a rare earth nucleus with N > 90. The upper edge of the bump moves to higher energies with increasing multiplicity up to $M\gamma = 27$. The observed angular distribution of the γ-rays confirmed the quadrupole character of the bump. At higher multiplicities a spike, with a stretched dipole character, at $\simeq$ 700 keV is observed. Despite the onset of a localized dipole transitions, the upper edge of the quadrupole bump continues to move to higher E_γ for higher multiplicities. The appearance of the dipole component occurs at the same multiplicity as the decrease in the slope of the entry line (fig. 2a) and thus explains the behaviour. Interestingly, the dipole component ($\sim$ 0.7 MeV) is located at about half the energy of the quadrupole component ($\sim$ 1.4 MeV).

In ^{160}Yb this observed change in the decay mode is even more pronounced. For M_γ up to 25 the spectra show a similar evolving bump (fig 3b), which is completely consistent with stretched E2 transitions at all E_γ, as seen from the anisotropies of the γ-rays shown in fig. 4a (M_γ = 16-19). Above $M_\gamma \simeq 25$ the γ-ray spectra show additional transitions localized at $E_\gamma \sim 650$ keV and that the quadrupole bump continues to evolve upward somewhat slower as M_γ increases. The dipole character of the transitions localized at $\sim$ 650 keV can clearly be seen from the anisotropies shown in

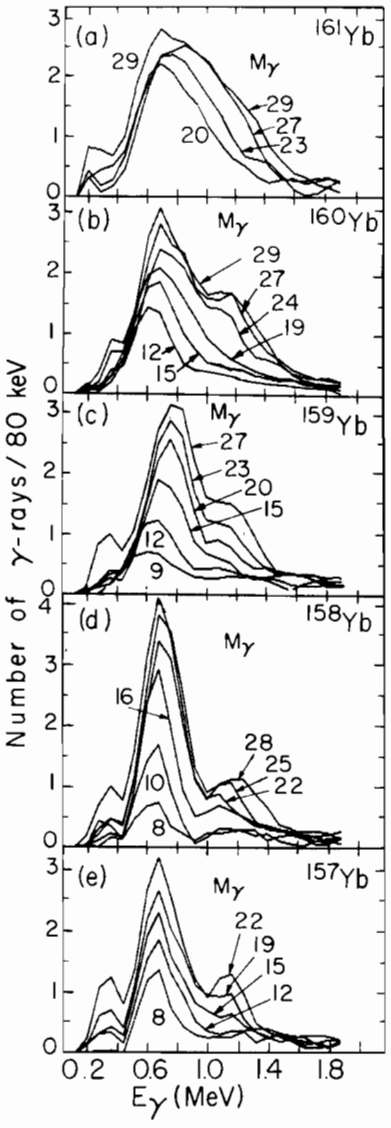

Fig. 3 Unfolded continuum γ-ray spectra of $^{161-157}$Yb for selected $M\gamma$ as indicated from the reactions: (a) ^{146}Nd(^{20}Ne,5n) at 136 MeV, (b) ^{146}Nd(^{20}Ne,6n) at 136 MeV and 149 MeV, (c) ^{146}Nd(^{20}Ne,7n) at 136 MeV and 149 MeV, (d) ^{146}Nd(^{20}Ne, 8n) and ^{144}Nd(^{20}Ne,6n) at 149 MeV, (e) ^{144}Nd(^{20}Ne,7n) at 149 MeV.

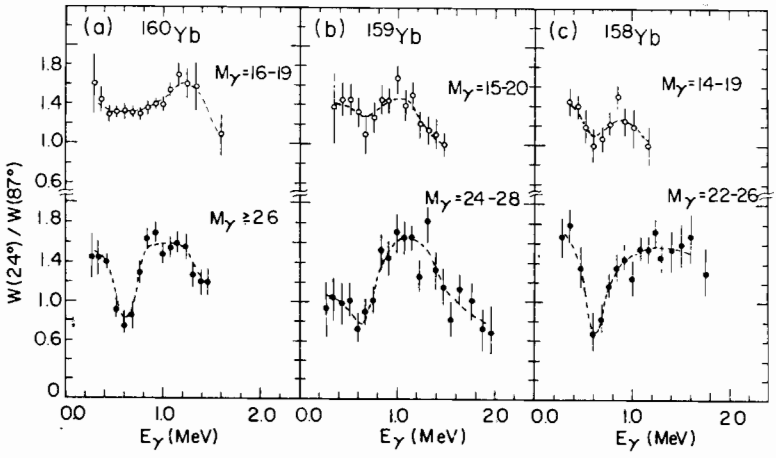

Fig. 4 Anisotropies of the continuum γ-rays in (a) ^{160}Yb, (b) ^{159}Yb, and (c) ^{158}Yb. The M_γ values indicated give the half maximum limits corresponding to the k gates used.

fig. 4a for $M_\gamma \geq 26$. An analysis of the difference spectra for succesively higher multiplicities, together with the angular distribution information, indicates a dipole to quadrupole ratio of 0.9 ± 0.2. This ammount of the dipole transitions accounts exactly for the observed decrease of the slope in the entry lines in figs. 2a and 2b. The constant slope of the entry lines above M ≈ 27 further suggests that the ratio of the dipole and the quadrupole transitions remains essentially constant up to highest observed multiplicities ∿ 32.

The multiplicity was connected to the nuclear spin using the observed γ-decay properties of the nuclei and the statistical model calculations discussed earlier. For multiplicities below the observed change in the slope of the entry line the rotational picture used in the calculations reproduces the entry state populations and the slopes of the entry lines well and thus the mapping for those multiplicities was taken from the calculated entry lines as a function of M_γ and of I using the formula $\langle I \rangle = (\Sigma\ I * R_X(I,M_\gamma))/(\Sigma\ R_X(I,M_\gamma))$, where $R_X(I,M_\gamma)$ is the calculated entry state distribution in (I,M_γ) space. For higher multiplicities the additional $\Delta I = 1$ transitions were taken into account by changing the M_γ to I conversion above the turning point by factor ∿ 0.75 corresponding to the equal dipole to quadrupole ratio.By using the maping described above the multiplicities where the onset of the new decay mode occur correspond to I ≈ 50 ($M_\gamma \approx 27$) and I ≈ 45 ($M_\gamma \approx 25$) for ^{161}Yb and ^{160}Yb, respectively.

The trend for the appearance of the dipole component at progressively lower spins as neutron number decreases continues in the lighter Yb isotopes as seen from the data in figs. 3 and 4. The onset of the new decay mode occurs at $M_\gamma \approx 23$ (I ≈ 42) for ^{159}Yb. An additional interesting phenomenon is observed in the data of ^{158}Yb. Entry lines for the population of ^{158}Yb (fig. 2c) show nearly the expected slope for $M_\gamma < 22$. At $M_\gamma \approx 22$ the slope of the entry line decreases and then at $M_\gamma \approx 28$ it increases, taking a value close to that of $M_\gamma < 22$. Two prominent features are apparent in the spectra from ^{144}Nd(^{20}Ne,6n)^{158}Yb and ^{146}Nd(^{20}Ne,8n)^{158}Yb reactions at 149 MeV shown in fig 3d. In this case a bump at E_γ ∿ 500 - 900 keV which evolves smoothly up to $M_\gamma \approx 20$ is seen. Above $M_\gamma \approx 22$ a second bump at higher energy with its upper edge reaching to ∿ 1.4 MeV at $M_\gamma \approx 28$ appears. The behavior of these bumps with increasing multiplicity together with the shape of the entry lines and the angular distribution data, provides a

consistent picture of the de-exitation of ^{158}Yb. The yrast decay sheme for ^{158}Yb is known up to 12^+ state and includes a cascade of stretched E2 transitions with energies from 358 keV to 683 keV[21]). The observed motion of the upper edge of the lower bump is consistent with the continuation of a predominantly quadrupole cascade up to $M_\gamma \simeq 20$ ($I \simeq 36$). Hovever,the angular distributions of the γ-rays from 500 to 800 keV for M_γ between 12 and 20 are less anisotropic than would be expected for pure stretched quadrupole radiation (fig. 4c) indicating the presence of some dipoles. It is also seen as a small difference in the slopes of the observed and calculated entry lines for ^{146}Nd(^{20}Ne,8n)^{148}Yb reaction at 149 MeV (fig. 2c). Furthermore below $M_\gamma \simeq 20$ the difference spectra for successive M_γ bins show that the additional γ-rays contribute not only to the upper edge of the bump but also to the region of the peak. Between $M_\gamma \simeq 15 - 20$ the contribution of the additional transitions expands from 0.5 MeV to 1.0 MeV. These features suggest a tendency toward an aligned-quasiparticle structure, characteristic of nuclei with small oblate deformation, between $I \sim 25 - 40$ for ^{158}Yb.

A sudden change in the behavior of the decay of ^{158}Yb is seen at $M_\gamma \simeq 22$ (fig. 3d), exactly where the decrease in the slope of the entry line occurs (fig. 2c). The contribution of the additional γ-rays between $M_\gamma \simeq 22 - 28$ are localized in two separate components,at the lower half of the intense bump and at $E_\gamma \sim 1.3$ MeV well above the upper edge of the intense bump. The angular distributions of the γ-rays between M_γ=22-26 show a clear dipole and quadrupole character for the lower and higher energy component, respectively, as seen from the anisotropies in fig. 4c. Based on the difference spectra, the angular distributions and the shape of the entry line the dipoles are estimated to be confined to a narrow region of 650 ± 100 keV. This data also indicates that 3 to 4 out of 6 transitions between $M_\gamma \simeq 22 - 28$ are dipoles. The quadrupole transitions are also localized to a region of about 100 keV wide and the centre of it moves slowly upward from ~ 1.2 to ~ 1.3 MeV as the multiplicity increases from 22 to 27. Thus the decay mode of ^{158}Yb between $M_\gamma \simeq 22 - 26$ ($I \simeq 40 - 48$) is the same as the decay mode of ^{159}Yb, ^{160}Yb and ^{161}Yb above $I \simeq 42$, 45 and 50, respectively. In addition another change in the decay mode of ^{158}Yb is observed at the highest multiplicities. The growth of the dipole component decreases sharply at $M_\gamma \simeq 27$ while the high energy quadrouple component continues to evolve up to highest multiplicities studied. This is also consistent with the increase in the slope of the entry line at $M_\gamma \simeq 27$ and the slope, characteristic for qadrupole radiation at $I \sim 50$, it shows at $M_\gamma > 27$.

The behavior of ^{157}Yb was investigated using the ^{144}Nd(^{20}Ne,7n) reaction at 149 MeV for the multiplicity range between 8 and 23. For this limited range of M_γ the behavior of the γ-decay is identical to that of ^{158}Yb as seen from fig. 3e. The aligned single particle character is oserved at $M_\gamma \simeq 12 - 18$ ($I \simeq 20 - 35$) and the onset of new decay modes characterized by localized dipole and quadrupole transitions occur at $M \simeq 21$ ($I \simeq 38$).

After the onset of the new decay mode the upper edge of the quadrupole bump develops exactly the same way in all isotopes evolving toward higher energies with increasing spin while they decay in a different way at lower spins. This quadrupole radiation is a new component not connected to the continuation of the low spin rotational spectrum as can be seen from the spectra of the lighter isotopes where the bump develops apart from the bump observed at lower spin. However, the effective moment of inertia calculated from the position of the edge of the bump and the associated spin is $\sim 150\ \hbar\ \mathrm{MeV}^{-1}$ and increases slightly with increasing spin. This behavior is close to the predictions of the rotating liquid drop model.

4. Discussion

From the data a systematic variation of the decay mode in the $^{157-161}$Yb isotopes is observed. This variation correlates with neutron number and nuclear spin. The variations of the decay mode are reflected as the onset of a strong dipole component located at half the energy of a quadrupole component that evolves in energy with increasing spin. The new decay mode appears at $I \simeq 38$, 40, 42, 45 and

50 in N = 87, 88, 89, 90 and 91 Yb isotopes, respectively. The decay spectra for ^{157}Yb and ^{158}Yb at I $\sim$ 20 - 35 suggest a behavior similiar to that of lighter N $\simeq$ 86 nuclei such as ^{152}Dy[22]) which is characteristic of particle aligned states found in slightly oblate nuclei.

Detailed systematic calculations of nuclear structure effects as a function of spin in these Yb isotopes, have been performed by Andersson et. al.[15]). The general features of their calculations can be used as a guide to possible interpretation of the changes observed in the decay modes of N = 87 - 91 Yb isotopes. Their results, combined with known pairing effects at low spin, for the nuclear shape and deformation as a function of angular momentum are shown in fig. 5. The results for odd-A isotopes were obtained by interpolation. Due to pairing effects at low spin (I $\lesssim$ 20) all the N > 86 Yb isotopes are prolate with $\varepsilon \simeq 0.1 - 0.3$. With increasing spin the deformation decreases, but the nuclei stay prolate ($\gamma \simeq 0^{\circ}$). At higher spins a sudden change to oblate shape is predicted for the lighter Yb isotopes. This change occurs at progressively higher spins with increasing neutron number. As the angular momentum further increases the nuclear shape develops back towards prolate shape via an intermediate triaxial shape. ^{162}Yb is predicted to be oblate only near I = 60 and ^{160}Yb is expected to become oblate at I $\sim$ 40 - 50 and to remain oblate up to spin $\sim$ 70. ^{158}Yb is predicted to become oblate at low spin and to evolve to triaxial shape above I $\simeq$ 50 .

In ^{157}Yb and ^{158}Yb the observed γ-decay indicates aligned single-particle behavior between I $\sim$ 20-35. This is just the structure which would be expected if these nuclei have the weakly deformed ($\varepsilon \simeq 0.1$) oblate shape predicted by the calculations. The $^{157-161}$Yb nuclei all have a similiar decay above I $\simeq$ 38 in the spin range where they are predicted to be oblate.This, in addition to the observed single particle character of ^{157}Yb and ^{158}Yb at lower spins (where they only are predicted to be oblate), indicates that the observed decay mode with localized dipole and quadrupole transitions is associated with an oblate nuclear shape. However, because of the localization of the dipoles near half the energy of the quadrupole radiation observed at the same multiplicities, it is obvious that transitions in collective bands are responsible for these γ-rays. The yrast states of an oblate nucleus, whatever its deformation, are most likely to be aligned quasiparticle states with spin vector along the symmetry axis. Thus these are K $\simeq$ I states upon which collective states could be built. According to theoretical investigations appreciable collectivity should not be expected for $|\varepsilon| < 0.25$, but could be important for larger deformations[23]). The exited states of these bands will not be yrast but could lie close to the yrast line. M1 radiation should in fact be favoured within these bands since according to the rotational model $B(M1) \propto K^2$ while $B(E2) \propto 1/K$.

From the arguments discussed in previous sections a possible explanation for the behavior of the decay modes observed in $^{157-161}$Yb can be found. The evidence for a transition to aligned single particle structure at low spin in ^{157}Yb and ^{158}Yb was observed as discussed earlier. This behavior is obviously connected with small deformations ($\varepsilon \simeq 0.1 - 0.2$). The new collective decay mode with localized M1 and E2 transitions, which can be connected with large basically oblate deformations ($\varepsilon \gtrsim 0.25$), appears at I $\simeq$ 38, 40, 42, 45 and 50 in ^{157}Yb, ^{158}Yb, ^{159}Yb, ^{160}Yb and ^{161}Yb, respectively. This suggests an evolution along $\gamma \simeq 60^{\circ}$ axis for ^{157}Yb and ^{158}Yb in the direction of increasing $|\varepsilon|$ between I $\simeq$ 20 and 40. Since the aligned quasiparticle states most favourably are the orbitals of highest available j above the closed shell the valence configuration tends to polarize also the core. Furthermore, when core-excitations are needed to increase the angular momentum the most favoured ones involve spherical holes below the shell gap and oblate particle states above the gap. Thus simply from the shell structure considerations, the oblate deformation continues to increase with increasing angular momentum just as for the rotating liquid drop. The A > 158 appear to undergo a transition to (or close to) the $\gamma = 60^{\circ}$ (oblate) axis with $|\varepsilon|$ already large enough to allow collective excitations.The spins at which the transition is observed as a function of $|\varepsilon|$ agree with the theory not only in qualitative trend but also quantitatively. According to the theoretical calculations all the Yb isotopes become unstable with respect to triaxial shapes at sufficiently high spin. Only in case of ^{158}Yb this change is predicted to occur

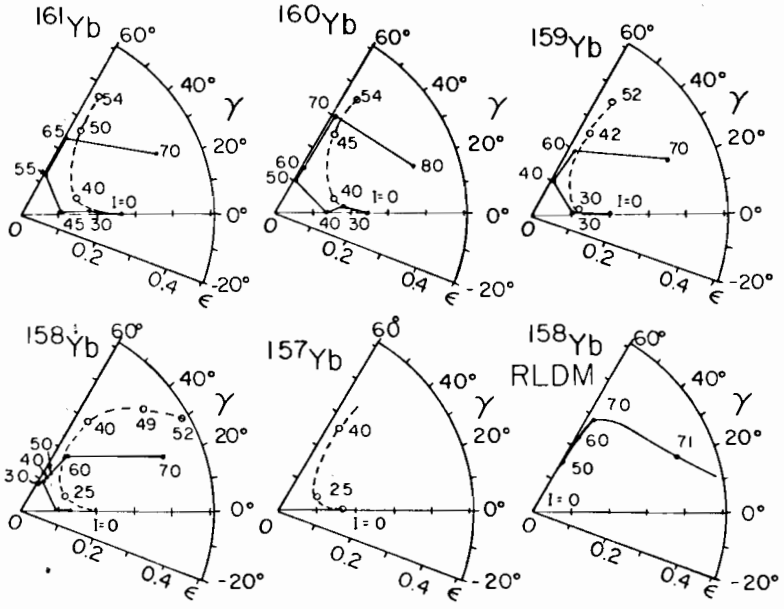

Fig. 5 Trajectories of equilibrium shapes in the (ε,γ) plane for N = 91 - 87 Yb isotopes. The solid lines are from the calculations in ref. [15]) (even-A) and interpolation from the calculations (odd-A). The dashed lines represent pictorically the shapes interpreted from the experimental data. The dots and open circles give the spin values demarking the trajectories.

at the spin range covered by the present experiments. Interestingly, ^{158}Yb is the only nucleus in which a disappearance of the dipole radiation was observed (at spin $\simeq$ 49), thus showing evidence for such change. This further strengthens the parallel between the observed data and the applied explanation.

In fig. 5 a path of the evolution of the Yb nuclei as a function of spin is summarized using the calculations of Andersson et. al. (solid line) as a guide. The smooth dashed curves in the figure present pictorically the evolution of the nuclear shapes using the deformations discussed earlier. The qualitative relationship between experiment and theory as a function of spin and neutron number is remarkable, except for two features. The calculations for ^{158}Yb predict constant ε between I = 20 - 40 but the data suggests an increase in ε along the γ = 60 axis for ^{157}Yb and ^{158}Yb, and in all the isotopes studied larger deformations for the oblate shapes at high angular momentum are suggested than the calculations predict. However, it should be noted that the calculations are made for the yrast configuration and the data reflects the properties of the states above the yrast line. Also possible small triaxiality could lower the required ε-deformation.

In the present analysis of the data only γ-ray multiplicity (no E^* selection) was selected. Thus at each M_γ the data presents an average of decay paths which begin almost 10 MeV above the yrast line. Nuclear structure effects from addition of single neutrons should not affect the decay at such high excitation. Yet a strong correlation of the decay mode with neutron number is observed. This indicates that the nuclear de-exitation approaches the yrast line rapidly, so that the bulk of the collective transitions which is observed occurs quite close to the yrast line. The fact that the γ-ray spectra below $E_\gamma \simeq 1.4$ MeV for a given I are independent of bombarding energy further strenghtens this interpretation.

This work was supported in part by the U.S. Department of Energy. Oak Ridge National Laboratory is operated by Union Carbide Corporation for the U.S. Department of Energy under contract W-7405-eng-26.

References

1) R.M.Diamond and F.S.Stephens, Ann.Rev.Nucl.Sci. 30 (1980) 85
2) A.Bohr and B.Mottelson,Phys. Scripta 10A (1974) 13; ibid. 24 (1981) 71
3) G.B.Hageman,R.Broda,B.Herskind,M.Ishihara,S.Ogaza and H.Ryde, Nucl. Phys. A245 (1975) 166
4) D.G.Sarantites,J.H.Barker,M.L.Halbert,D.C.Hensley,R.A.Dayras,E.Eichler, N.R.Johnson and S.A.Gronemeyer,Phys.Rev. C14 (1976) 2138
5) J.O.Newton,I.Y.Lee,R.S.Simons,M.M.Aleonard,Y.ElMasri,F.S.Stephens and R.M.Diamond,Phys.Rev.Lett. 38 (1977) 810
6) D.L.Hills,J.D.Garrett,O.Christensen,B.Fernandez,G.B.Hageman,B.Herskind, B.B.Back and F.Folkmann,Nucl. Phys. A325 (1979) 216
7) F.Folkmann,J.D.Garrett,G.B.Hageman,M.N.Harkeh,B.Herskind,D.L.Hills,SOgaza, H.Emling,E.Grosse,D.Schwalm,R.S.Simons and P.O.Tjøm,Nucl. Phys A361 (1981) 242
8) PChowdhury,J.Borggreen,T.L.Khoo,I.Ahmad,R.K.Smither,S.R.Faber,P.J.Daly, C.L.Dors and J.Wilson,Phys.Rev.Lett. 47 (1981) 778
9) O.Andersen,J.D.Garrett,G.B.Hageman,B.Herskind,D.L.Hills and L.L.Riedinger, Phys.Rev. Lett. 43 (1979) 687)
10) T.L.Khoo,J.dePhys. C10 (1980) 9
11) S.Cohen,F.Plasil and W.J.Swiatecki,Ann. of Phys. 82 (1974) 5
12) L.L.Riedinger,Proc. of the Nuclear Physics Workshop,Trieste,1981
13) I.Ragnarson,T.Bengtsson,G.Leander and s.Åberg,Nucl. Phys. A347 (1980) 287
14) R.Bengtsson,S.E.Larsson,G.Leander,P.Möller,S.G.Nilson,S.Åberg and Z.Szymanski,Phys. Lett. 57B (1975) 301
15) G.Andersson,S.E.Larsson,G.Leander,P.Möller,S.G.Nilsson,I.Ragnarsson,S.Åberg, R.Bengtsson,J.Dubek,B.Nero-Pomorska,K.Pomorski and Z.Szymanski, Nucl. Phys. A268 (1976) 205
16) S.Åberg,Phys. Scripta 25 (1982) 23
17) M.Jääskeläinen,D.G.Sarantites,R.Woodward,F.A.Dilmanian,J.T.Hood,R.Jääskeläinen, D.C.Hensley,M.L.Halbert and J.H.Barker,Nucl. Instr. Meth. (in press)
18) D.G.Sarantites,M.Jääskeläinen,R.Woodward,F.A.Dilmanian,D.C.Hensley,J.H.Barker, J.R.Beene,M.L.Halbert and W.T.Milner,Phys. Lett. B (in press)
19) Code JULIAN,M.Hillman and Y.Eyal (unpublished);modification PACE by A.Gavron, Phys. Rev. C21 (1980) 230
20) J.Wilczynski,K.Siwek-Wilczynska,J.van Driel,S.Gonggrijp,D.C.J.M.Hageman, R.V.F.Janssens,J.Lukasiak and R.H.Siemssen, Phys.Rev.Lett 45 (1980) 606
21) W.Troutman,D.Proetel,O.Häusser,W.Hering and F.Riess, Phys. Rev. Lett. 35 (1975) 1694
22) T.L.Khoo,R.R.Smither,B.Haas,O.Häusser,H.R.Andrews,D.Horn and D.Ward, Phys. Rev. Lett. 41 (1978) 1027
23) C.G.Andersson and G.Leander,Nordic Conference on Nuclear Physics, Lysekil,Sweden 1979